

# Structural Testbed Design and Testing with Controlled Nonlinearities

Steven M. Whitican, MAG Automotive LLC, Sterling Heights, Michigan

Timothy J. Copeland, m+p international, Verona, New Jersey

A structure was developed to provide a realistic test bed for high-channel-count linear and nonlinear modal analysis. The goal was to model and construct a linear structure to serve as a platform to introduce controlled nonlinearities. These nonlinearities are designed to mimic airframe nonlinear structures including ailerons, engine mounts, payload and bomb mounts including wingtip stores. The model was constructed and modeled with several pretest analyses performed to identify a minimum sensor configuration that could correlate the modes of interest. Impact testing validated the sensor configuration prior to testing with 144 input channels and multiple sources. Correlation was accomplished and resulted in an updated FE model. Once this baseline was completed the introduction of controlled nonlinearities allowed application of the existing and emerging nonlinear modal analysis tools. This article is a description of the construction, testing and correlation of the structure with a nonlinearity evaluation.

The prototype model shown in Figure 1 was developed to provide a good dynamic response with flexibility for bolted components allowing nonlinearities to be introduced for additional testing. Many possible designs were evaluated but ease of construction and visual familiarity of a fighter was decided upon. The final dimensions were chosen to allow placement of a large number of accelerometers that serves to duplicate actual testing requirements.

After modeling this prototype, a preliminary finite-element analysis (FEA) was accomplished to ensure the structure would meet our requirements. The primary goal was to have well defined wing modes as the plan to introduce controlled nonlinear components focused on the wings. In addition, using bolts to fasten the wings to the fuselage provided another area of possible nonlinearity and provided for some portability.

## Model Construction

Steel was chosen for the model based on availability and material properties. Overall size was determined to be a 40-inch wing span and a 52-inch length with a weight of 65 lbs. The wings and central stabilizer were 3/16-inch thickness and profiled on a water jet. The model plane's central fuselage tube had a 4-inch outer diameter with a wall thickness of 1/8 inch. The vertical stabilizer is the only profiled piece continuously welded directly to the fuselage. Angle irons were welded to the fuselage for the attachment of the wings to prevent them from undergoing thermal distortion due to the weld. The angle irons were continuously welded across the top, where there was line-to-line contact with the fuselage and skip welded across the bottom where there was a gap. Figure 2 shows the completed and painted structure suspended for impact testing.

## Modeling

All components (wings, fuselage, and vertical stabilizer) were modeled with quadratic-shell elements. The mesh size suggested by the preprocessor was used. Figure 3 shows the initial finite-element model.

Welds were modeled with beam elements of the approximate geometry of the weld. The initial stiffness was based on Young's Modulus for steel. Contact between the bodies were modeled with linear springs, also with the Young's Modulus of steel. Bolts were modeled with beams, point masses, and rigid connectors, with the connectors allowed to attach at mid-nodes.

Several solutions were computed with the model. The frequency band of interest was between 0 and 250 Hz. First the unconstrained

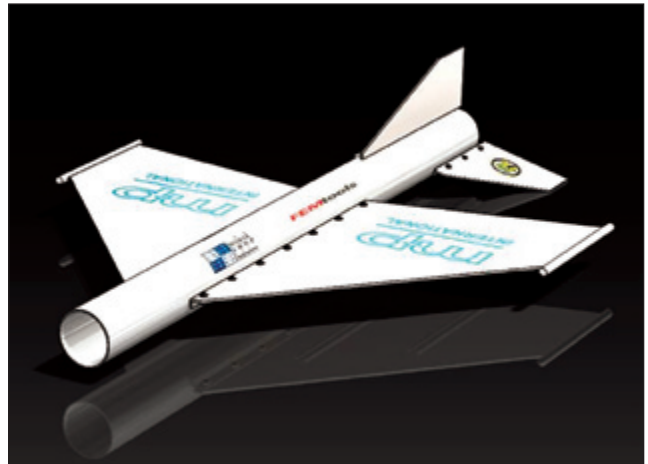


Figure 1. Prototype 3D model.



Figure 2. Test article painted and ready for impact testing.

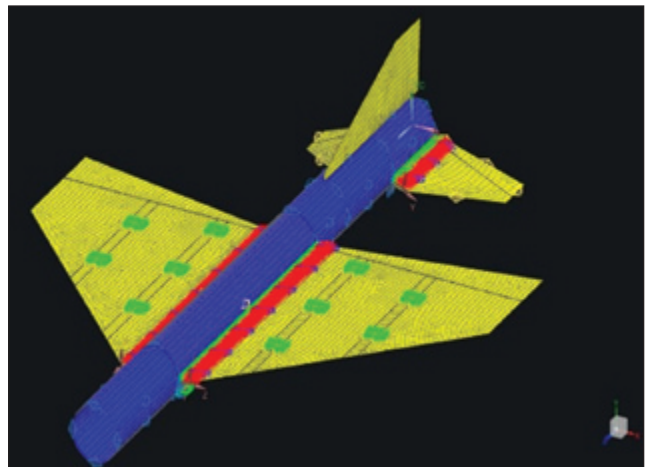


Figure 3. Initial finite-element model (FEM).

real normal modes were calculated and studied in anticipation of how the real structure would behave. Response locations were also picked from this initial simulation for an impact test of the prototype structure. Frequency response functions (FRFs) were also

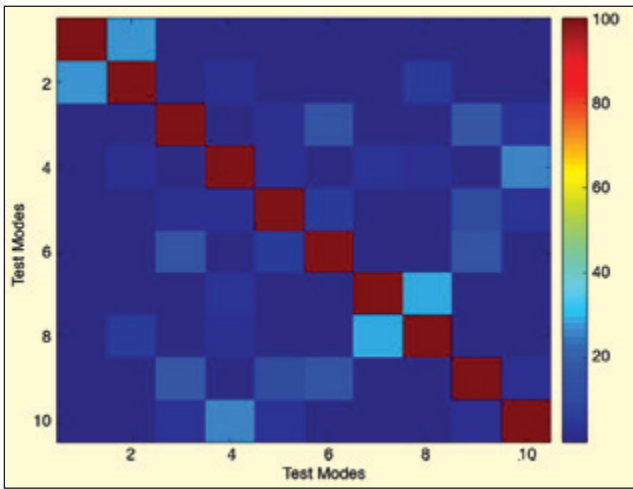


Figure 4 Auto MAC automated sensor placement, 18 triaxial accelerometers.

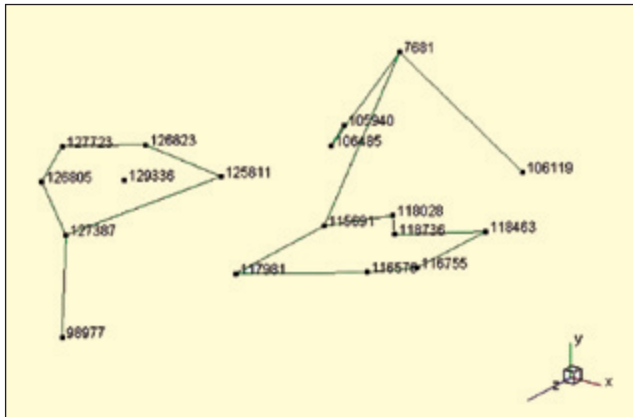


Figure 5 Pre-test analysis-driven modal model (18 triaxial accelerometers).

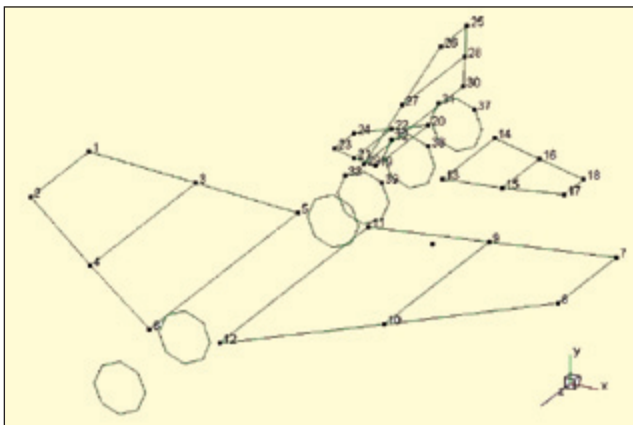


Figure 6 Preliminary modal model used for initial impact testing.

calculated at an assumed location where modal exciters would be attached to the structure. The FRFs were computed on a modal basis with 1% critical damping assumed in the band of interest.

### Test Plan

The primary goal of the testing was to provide modal models to correlate and update the FE model. Additional requirements were to improve ground vibration testing and nonlinearity detection. An outline of the test plan is provided below.

- Pretest analysis to locate transducers and determine best methods based on analysis results.
- Impact testing for mounting evaluation, quick look results and nonlinearity checks.
- Shaker testing with up to 6 shakers and up to 144 accelerometers.
- Evaluate linearity of baseline structure by varying the force patterns and levels.
- Correlate a linear FEM and update the model.

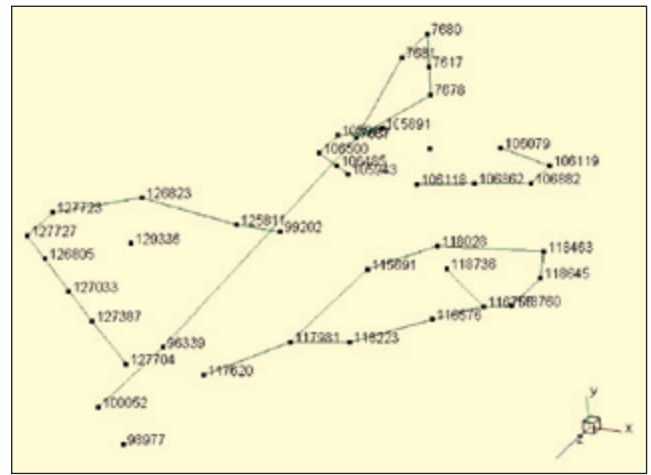


Figure 7. Expanded modal model (40 triaxial accelerometers).

- Introduce controlled nonlinearity and refine techniques for detection and identification.

### Pretest

The goal of pretest analysis was to provide guidance on where to instrument the structure based on certain requirements. NAS-TRAN was the solver used to calculate preliminary mode shapes and FRFs. Op2 files were then imported to FEMTools for pre-test analysis and correlation. The first modal model was developed on the assumption that 64 channels of acquisition were available. The software was requested to generate locations for 18 triaxial accelerometers so that the off-diagonal modal assurance criterion (MAC) was less than 30%. The auto MAC calculated from the experimental data is shown in Figure 4. The maximum off-diagonal was approximately 29%. The pretest analysis with 18 triaxial accelerometer locations is shown in Figure 5.

### Impact Testing

The initial modal model is shown in Figure 6. The primary goal was to characterize the structure, the mounting method and determine construction and assembly quality. This model did not take into account the pretest analysis accelerometer locations, since it was performed before the analysis was available. This is representative of modal models that are created prior to access to the FE model, and the locations are selected based on a visual aesthetic rather a mathematical basis.

The structure was suspended by elastic cords fore and aft of the fuselage. The elastic cords are connected to the structure with twine, which adds neither mass nor stiffness to the structure. This matches the support technique during the later shaker testing.

Two triaxial 10 mV/g accelerometers were cemented to the structure at either wing tip shown at point 1 and point 7 in Figure 6. Surface normal readings were kept and used for curve-fitting, and two references were used for extracting modal parameters. A soft plastic tip was used based on the low frequency range and the light damping of the linear structure. Data were captured and parameter estimation completed. These data were compared with those obtained later when the structure was moved to the testing location and instrumented. This determined that the fully instrumented and supported structure was not being mass loaded by the accelerometers or affected by the new mounting setup.

### Shaker Testing

The structure was moved to the University of Illinois Linear/Nonlinear Laboratory and suspended for unconstrained testing from a cantilevered I beam. It was hung from a set of elastic straps fore and aft of the fuselage. The elastic straps were combined so that the rigid-body modes were less than one-tenth of the first flexible body mode. Suspension frequency was determined by applying an initial displacement to the structure and recording the ring down and observing the primary low-frequency component.

The structure was instrumented based on the pre-test analysis

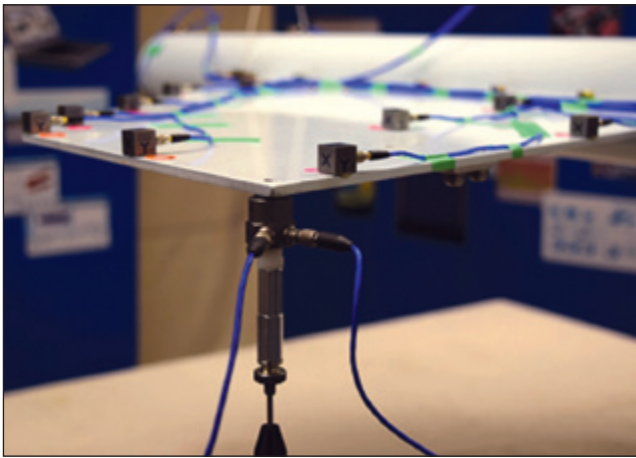


Figure 8. Impedance head – excitation location.

minimum requirements with 18 tri-axial accelerometers. This involved 54 input channels of acquisition, not including excitation or output channels. This baseline configuration was supplemented with an additional model to increase the channel count to use the available system and sensor maximum as well as provide increased geometric resolution for later nonlinearity study. This second model added 22 more accelerometers (40 total) and an input channel count of 120, as shown in Figure 7.

In both cases, the 18 or 40 triaxial accelerometers were mounted with hot glue. This was evaluated and provided excellent transmission in the frequency range of interest. The experimental setup is shown on the front cover of this issue.

Impact testing with a soft rubber tip was done to ensure all accelerometers were working and placed correctly. Single degree of freedom curve fitting was performed on a couple of the lower modes to ensure consistency with the pretest impact testing.

Multiple shaker configurations were used and the first tests utilized a 100-pound shaker on a single wingtip. Figure 8 shows the excitation location and attachment to the wing. An impedance sensor was used and provided both force and acceleration output. This is the signal that is used as the driving point. Impedance heads were stud mounted to the structure at the locations where the shakers were connected.

Burst random excitation at a low level was used with 50 averages. The goal was to input sufficient energy at all locations and obtain a linear response. Swept sine was used including the newly developed high-rate swept sine analysis using the complex spectrum. This enabled much quicker first-look sweeps without frequency bias. Stepped-sine excitation was used for most configurations. A secondary 100-pound shaker was added to the other wing tip to investigate effects on the force patterns using phase relationships. Dual shakers were also used for higher force level excitation in linearity checks and during the nonlinear component testing phase.

Normal mode tuning was used with dual and single 100-pound shaker configurations. This special case of sine excitation enabled tuning the structure to ensure a specific phase relationship between inputs and output. Both automatic and manual tuning were used with adjustment of the frequency and phase of each shaker. This configuration also allowed overlay of the FRFs with easy amplitude adjustment to check for nonlinearities.

### Parameter Estimation

The primary excitation used for correlation was a single 100-pound shaker and stepped sine. The data shown in Table 1 were curve fit with both polyreference time and frequency-domain, curve-fitting algorithms. Mode shapes shown in a subsequent section of this article were computed using the enhanced polyreference time domain.

### Model Analysis Correlation (MAC)

The correlation is shown for the 18 accelerometer model, and it can be seen that this model was more than adequate for the modes of interest. MAC results are shown in Figure 9.

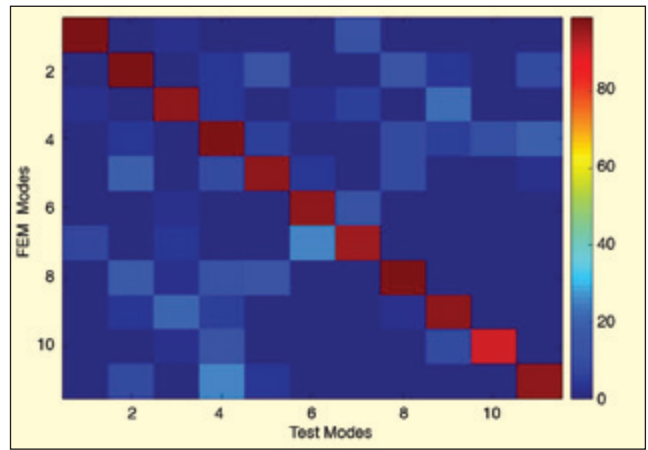


Figure 9. Pre-model-update modal assurance criterion (MAC).



Figure 10. First flexible-body mode shape.

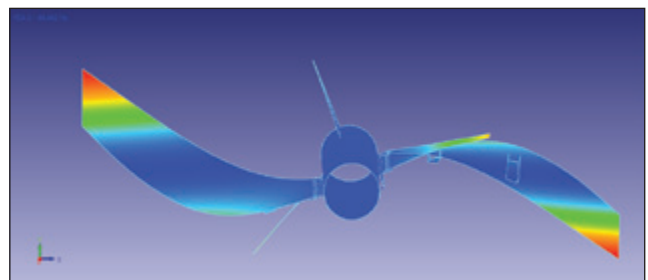


Figure 11. Second flexible-body mode shape.

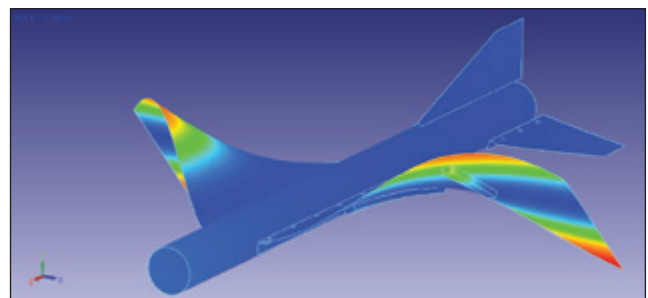


Figure 12. Third flexible-body mode shape.

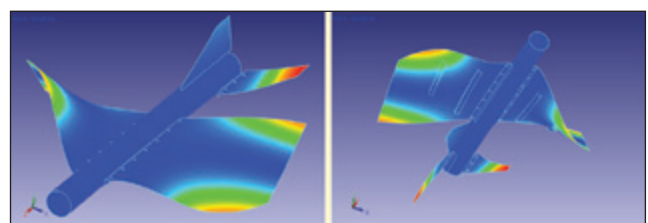


Figure 13. Fourth flexible-body mode shape.

Mode 10 possesses the lowest MAC at 92%. Otherwise, in the band of interest, the FEM correlates well with the experimental model. When Mode 10 is investigated for removing non-consistent DOFs, the primary DOFs removed are those out of the direction of excitation.

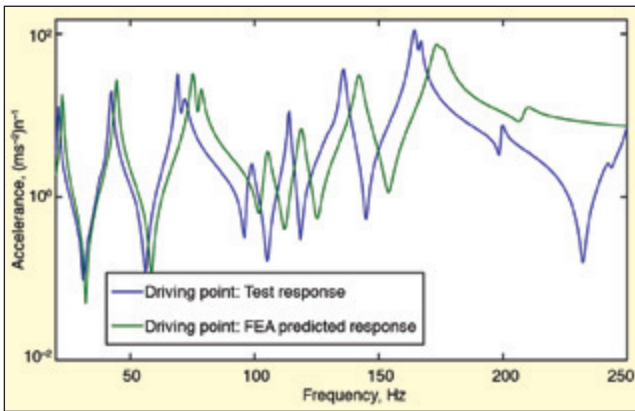


Figure 14. Comparison of calculated vs. measured driving point FRFs.

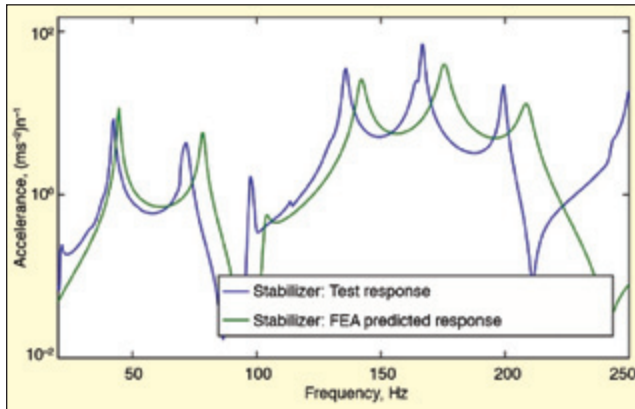


Figure 15. Comparison of calculated vs. measured FRFs at central stabilizer.

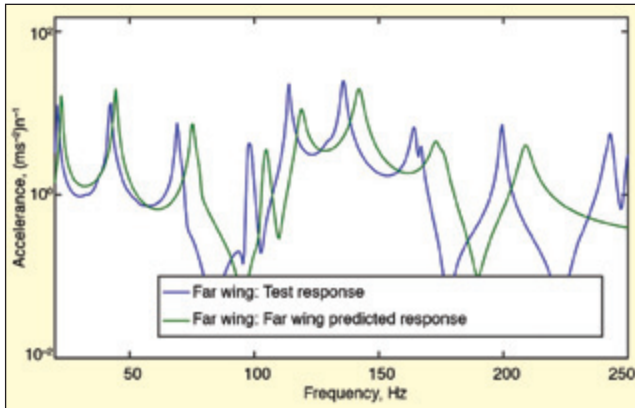


Figure 16. Comparison of calculated vs. measured FRFs at wing tip opposite driving point.

The first four mode shapes are shown in 10 through Figure 13. All of the modes in the range of interest involve primary displacement in the wings and stabilizer. The fuselage tube does not participate in the lower order modes.

Table 1. Extracted modal parameters from primary excitation.

Mode Number	Frequency, Hz	Damping Ratio, %
1	21.12	1.05
2	42.28	1.03
3	69.15	0.59
4	71.65	1.56
5	97.32	0.50
6	98.68	0.76
7	113.85	0.43
8	135.81	0.61
9	164.33	0.61
10	166.74	0.36
11	199.39	0.33

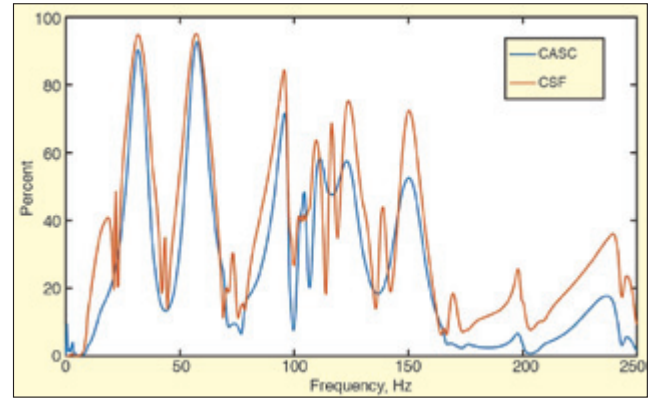


Figure 17. FRF correlation metrics in band of interest.

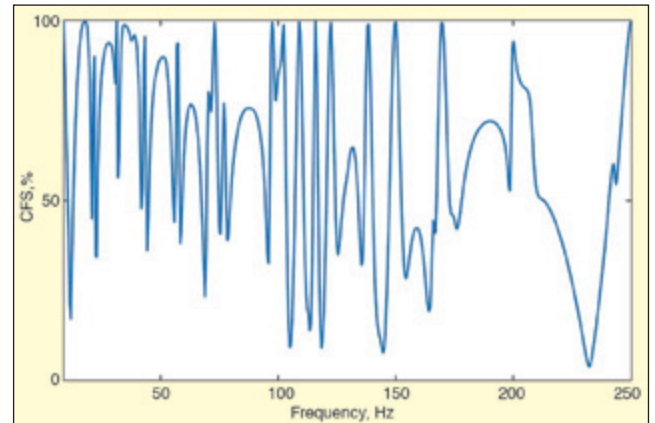


Figure 18. FRF correlation metric comparing driving point only.

Comparing mode shapes, however, is half of the story in this case and proves to be optimistic. Though the mode shapes match well, there is some discrepancy between the measured and calculated FRFs. Measured and calculated FRFs are overlaid in Figures 14-16.

In all instances, the FEM is more stiff than the experimental structure. The experimental structure was put on a scale and found to be 65.2 lbs., while the FEM calculates the weight to be 65.54 lbs.

Figure 17 displays the FRF correlation metrics for all paired FRFs. The FRFs correlate well at the first couple modes and then drop off for those of higher order. The driving points compare well when the cross-signature scale factor (CSF) is calculated based solely on the driving-point measurements shown in Figure 18.

Spikes in the CSF are due to crossings between the FRFs and are ignored in the analysis of the plots. Table 2 compares the test natural frequencies to the FEM natural frequencies. Based on the overall model rigidity and the FEM overpredicting natural frequencies, the global Young's modulus will be investigated during the next phase of model updating.

### Controlled Nonlinearities

Several concepts have been developed to introduce controlled nonlinearities that replicate operational configurations. The bolted structure allows introducing variability in the wing-to-fuselage interface. Underwing attachments were designed to enable stores or engine connections as shown in Figure 19. The first to be implemented during this testing is a device to mimic aileron flutter and is shown in Figure 20.

Various levels of excitation were applied to the structure by the single shaker on the opposing wing tip. Sine sweeps were conducted with the data recorded as a time history for analysis to capture the nonlinearity in the time domain. The flexure was configured so that with 2 N excitation, it did not rattle against the structure. That way it was only acting as a mass load. With 4 N excitation, the flexure buzzed against the structure at a few of the flexible body modes. At 6 N excitation, the flexure buzzed against the structure at all flexible body modes. Figures 21 and 22 compare



Figure 19. Damping material used to attach payloads to wings at hard points.



Figure 20. Flexure used to approximate aileron flutter.

the time traces from the accelerometer mounted on the wing just above where the flexure impacted.

The traces shown are the enveloped data for clarity. It is clear from Figure 21 that there is not much difference between flexure and no flexure. However, Figure 22 shows the dramatic difference. The impacting flexure excites the higher-order modes of the structure. This is shown another way in Figures 23 and 24, where the frequency is included in the plots as a color map.

## Summary

A testbed structural model was designed, modeled, tested and correlated. This structure was designed to incorporate realistic, controlled nonlinearities. Current, evolving and emerging linear and nonlinear technologies have been applied. Ongoing research will result in further discoveries and insight that we look forward to sharing. Additional nonlinear elements and techniques will be the focus of further publications.

Table 2. Comparison of natural frequencies, measured vs. calculated.

Mode No.	Initial NX		5N Swept-Sine Excitation, 100-lbf Shaker	Diff., %
	NASTRAN Model, Hz			
1	22.94	21.12	7.93	
2	44.98	42.28	6.00	
3	75.81	69.15	8.79	
4	79.56	71.65	9.94	
5	106.42	97.32	8.55	
6	108.85	98.68	9.34	
7	120.96	113.85	5.88	
8	143.4	135.81	5.29	
9	174.3	164.33	5.72	
10	177.20	166.74	5.91	
11	203.79	199.39	2.16	

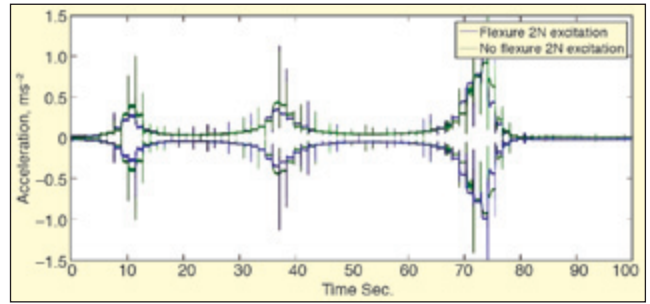


Figure 21. Comparison of time history with and without flexure, 2 N excitation.

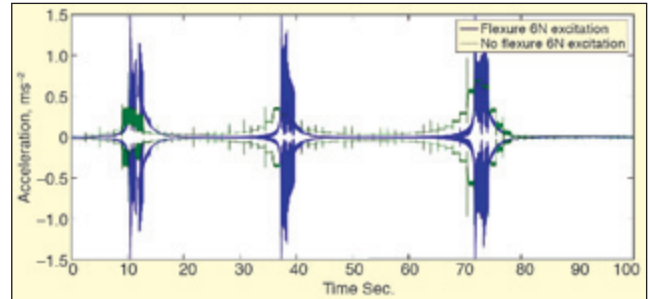


Figure 22. Comparison of time history with and without flexure, 6N excitation.

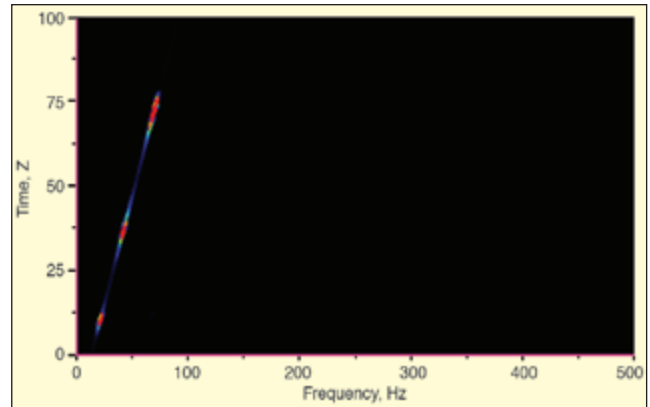


Figure 23. Time – frequency plot, 6 N excitation without flexure.

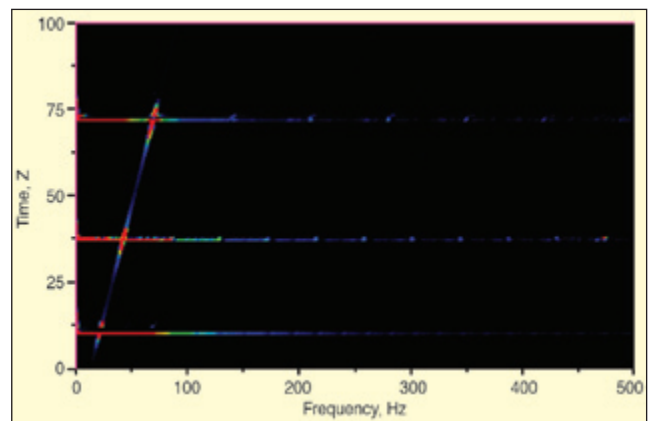


Figure 24. Time – frequency plot, 6 N excitation with flexure.

Our primary partners for this effort included m+p international (providing experimental modal software and a 144 input, 6 output modal system), FEMTools (providing pretest, correlation and model updating) and the Linear/Nonlinear Modal Analysis group at University of Illinois (providing facilities and nonlinear modal methods and test support). Instrumentation support was provided by The Modal Shop. 

The author can be contacted at: [tim.copeland@mpina.com](mailto:tim.copeland@mpina.com).